frontiers in Energy Research

ORIGINAL RESEARCH
published: 31 July 2018
doi: 10.3389/fenrg.2018.00064

Insight Into the Formation of Lithium Alloys in All-Solid-State Thin Film Lithium Batteries

Damian Goonetilleke[1], Neeraj Sharma[1], Justin Kimpton[2], Jules Galipaud[3,4], Brigitte Pecquenard[3,4] and Frédéric Le Cras[5]*

[1] School of Chemistry, University of New South Wales, Sydney, NSW, Australia, [2] Australian Synchrotron, Clayton, VIC, Australia, [3] Centre National de la Recherche Scientifique, University of Bordeaux, ICMCB, UPR 9048, Pessac, France, [4] Bordeaux INP, ICMCB, UPR 9048, Pessac, France, [5] CEA, LETI, Université Grenoble Alpes, Grenoble, France

Solid-state thin film batteries utilize electrode and electrolyte components which are nanometers or micrometers thick, enabling the production of novel devices with new form factors. Here, *in situ* X-ray diffraction is used to carry out the first study of a solid-state thin film lithium-ion battery containing a solid-state LiPON electrolyte and Bi negative electrode. The structure-electrochemistry relationships in the Li-Bi system are revealed and details of cell construction, data collection, and data analysis is presented to guide for research.

Keywords: solid-state battery, *in situ*, X-ray diffraction, structure-properties relationships, electrochemistry, electrode materials, thin-film

OPEN ACCESS

Edited by:
Jian Liu,
University of British Columbia Okanagan, Canada

Reviewed by:
Qian Sun,
University of Western Ontario, Canada
Biqiong Wang,
General Motors, United States

****Correspondence:***
Neeraj Sharma
neeraj.sharma@unsw.edu.au

Specialty section:
This article was submitted to Energy Storage, a section of the journal Frontiers in Energy Research

Received: *20 February 2018*
Accepted: *14 June 2018*
Published: *31 July 2018*

Citation:
Goonetilleke D, Sharma N, Kimpton J, Galipaud J, Pecquenard B and Le Cras F (2018) Insight Into the Formation of Lithium Alloys in All-Solid-State Thin Film Lithium Batteries. Front. Energy Res. 6:64. doi: 10.3389/fenrg.2018.00064

INTRODUCTION

All-solid-state microbatteries are an interesting development of conventional Li-ion batteries (LIBs), which operate in the same potential window and by similar reaction mechanisms. All-solid-state thin film lithium batteries (microbatteries) are becoming an essential component of emerging autonomous miniaturized electronic devices, allowing a maximized integration of their power source. Microbatteries are electrochemical cells in which thin films of the different cell components are stacked by various deposition techniques to form a functional electrochemical device, with individual layers having thicknesses ranging from tens of nanometers to a few micrometers. Typically, thin film battery systems consist of crystalline lithium intercalation compounds as the cathode, and metallic lithium negative electrodes (lithium thin film battery) or inorganic compounds in which the initial charge is used to form a negative electrode by lithium plating ("lithium-free thin film batteries") (Dudney and Neudecker, 1999; Bates et al., 2000). Thin films are generally prepared by vacuum deposition techniques such as sputtering or evaporation, which are already under widespread use in microelectronics fabrication (Kanehori et al., 1983; Dudney and Neudecker, 1999). The patterning of each material level, from the current collectors to the encapsulation layers, can be achieved either by shadow masking or by photolithography, allowing for customizable footprints with areas ranging from mm^2 to cm^2.

In thin film batteries, where diffusion lengths are minimized, solid-state electrolytes are favorable. Solid-state electrolytes are inherently advantageous over liquid electrolytes in terms of safety and handling thanks to their electrochemical, mechanical and thermal stability (Takada, 2013; Teng et al., 2014). Issues with capacity fade caused by the formation of a solid-electrolyte interface (SEI) are also avoided by using a solid-state electrolyte. This contributes to the cell

achieving a long calendar life, good capacity retention and stable electrochemical response (Bates et al., 2000; Fleutot et al., 2011; Cras et al., 2015). Electrochemical stability of solid-state electrolytes typically over a wider voltage window also allows for cells to operate at high voltages enabling higher energy densities to be achieved. Further, parasitic electrochemical reactions between the electrolyte and electrode are drastically reduced, if not suppressed (Bates et al., 1994).

Another useful asset of these cells is their 2D design, which can minimize large changes in the volume of the electrodes during (de-)lithiation (Zhao et al., 2015). Deposition techniques allow for a large variety of electrode materials to be used, from amorphous to crystalline, from thermodynamically stable to metastable forms, and from simple to complex multi-phase compounds. The thickness of the layers can also be finely controlled which can be useful to counterbalance low ionic/electronic conductivity. Electrode materials that can be prepared by sputtering or by pulsed laser deposition are indeed numerous and include well-known intercalation materials $LiCoO_2$ (Neudecker et al., 2000; Yoon et al., 2013), $LiMn_2O_4$ (Jones et al., 1994), $LiNi_{0.5}Mn_{1.5}O_4$ (Xia et al., 2007), $LiFePO_4$ (Bajars et al., 2011), V_2O_5 (West et al., 1992), conversion reaction materials FeS_2 (Pelé et al., 2015), CuO (Pecquenard et al., 2014), and pure or mixed Li-alloying materials (Dimov, 2009). In bulk battery systems, the use of lithium alloy negative electrodes has generally been avoided due to the significant volume changes which occur during the alloying process as a result of lithium insertion/removal (Besenhard et al., 1997). However, the high packing density of metallic lithium and lithium alloys makes it attractive to re-consider the use of lithium alloy negative electrodes for thin film batteries, where the volume change will not be nearly as significant as the bulk, and the increased specific capacity could be especially useful. A number of lithium binary alloy systems have been explored (Massalski et al., 1986), including Li-Al (Yao et al., 1971; Bang et al., 2001), Li-Si (Wen and Huggins, 1981), Li-Sn, and Li-Cd among others (Huggins, 1999). The high-packing density achieved when lithium is inserted into the metallic lattice is favorable for achieving better specific and volumetric capacities compared with lithium intercalation into carbonaceous materials (Besenhard et al., 1997).

Several systems using a lithium alloy negative electrode have been reported to date (Besenhard et al., 1997; Huggins, 1999; Bang et al., 2001; Zhang, 2011). In particular, Bi is an interesting candidate for use in thin film batteries for powering new, emerging microelectronics devices (Crosnier et al., 2001). Moreover Bi, which is a non-toxic material, has a high sputtering yield allowing the growth of several hundred nanometer thick thin films in a limited period of time. Li-Bi alloys form at relatively low potentials (0.8–0.6 V) which avoids electrochemical activity from other cell components vs. lithium (Crosnier et al., 2001; Xianming et al., 2002). Bi also offers a good theoretical specific capacity of 385 mAh g^{-1}, which is comparable to that of graphite (372 mAh g^{-1}) (Zhang, 2011), and a high volumetric capacity of 3,800 mAh cm^{-3}. The galvanostatic cycle curve of Bi vs. Li^+/Li is in agreement with the phase diagram, displaying two discharge plateaus corresponding to the formation of an LiBi phase, followed by the formation of Li_3Bi upon further Li insertion. Recently, it has also been clearly demonstrated that lithium binary alloy systems, especially Li-Si, may have a great interest in all-solid-state thin film configuration despite the large volume variation (300 % from Si to $Li_{15}Si_4$) occurring during Li insertion (Phan et al., 2012).

Several *in situ* structural studies of LIB systems have been carried out using both synchrotron X-ray diffraction (XRD) and neutron powder diffraction (NPD) (Sharma and Peterson, 2012; Hu et al., 2013; Pang et al., 2015; Sharma et al., 2015a; Goonetilleke et al., 2017). These studies allow the structural changes which take place in active materials to be related to the devices' electrochemical activity in real-time. While most *in situ* structural studies have focused on conventional LIBs using a liquid electrolyte (Sharma et al., 2015b), *in situ* structural characterization of a thin film battery utilizing a polymer electrolyte has been reported (Gustafsson et al., 1992). Solid-state batteries are ideal for diffraction studies as the absence of a liquid electrolyte and amorphous components such as separators removes large background contributions. Thus, considering their excellent electrochemical behavior, their versatility in terms of materials and their simple design, 2D all-solid-state thin film lithium microbatteries appear as promising devices to carry out *in situ* structural studies of various electrode materials. *In situ* and/or *operando* characterization of electrode materials operating in all-solid-state cells are rare. They mainly focus on chemical depth profiling by means of neutron techniques (Oudenhoven et al., 2011; Wang et al., 2017) or chemical analysis of solid-solid interfaces by means of scanning tunneling electron microscopy-electron energy loss spectroscopy (STEM-EELS, (Ma et al., 2016; Wang et al., 2016; Gong et al., 2017). To our knowledge, no *in situ* structural characterization has been carried out by X-ray diffraction on ceramic all-solid-state batteries so far.

We focused our study on the following stack: Bi | LiPON | Li, because it constitutes a model stack for *in situ* analysis, Bi being a heavy element and a crystalline material (well-adapted for X-ray analysis) and a potential candidate to replace Li as a negative electrode in all-solid-state thin film batteries. We report for the first time an *in situ* X-ray diffraction study of Bi/LiPON/Li all-solid-state cells. This preliminary study was achieved to follow the formation of lithium alloys during cycling of the cell.

EXPERIMENTAL

Cell Design

As all-solid-state thin film batteries do not contain any liquid, conductive additives or polymeric binders, their format is thus well suited for *in situ* diffraction studies (Zhou et al., 2013). Nevertheless, particular attention was devoted to the cell design considerations to ensure high quality diffraction data, including thickness of the electrode and electrolyte films, thickness and nature of substrate and encapsulation layers and surface and positioning of the cells on the substrate and the sample holder. As detailed below, the thickness of the active material is about a few hundred nanometers. A LiPON electrolyte (Bates et al., 1992) was chosen as it is an amorphous solid-state electrolyte for lithium ion batteries that

induces little-to-no scattering. This electrolyte offers high ionic conductivity and chemical stability against metallic lithium, which has led to its reported application in several solid-state LIB systems (Dudney, 2005; Jacke et al., 2010; Senevirathne et al., 2013). The thickness of substrate and encapsulation layers can contribute to a reduction in cell performance. Both were slimmed down as much as possible while keeping sufficient mechanical properties.

Four 9 × 9 mm^2 all-solid-state cells were prepared on thin glass substrate (50 µm thick, AF32 borosilicate glass, Schott Gmbh) by ICMCB and CEA in a chamber connected to a glove-box. The deposition of all levels of the stack was made through a shadow mask to localize each layer. A 200 nm Cr thin film was first deposited by sputtering to favor the adhesion of Bi thin film on the glass substrate. The Bi (250 nm) thin film was grown by radiofrequency sputtering under Ar on the Cr current collector. The Li-Bi binary diagram displays two definite compounds LiBi and Li_3Bi (Sangster and Pelton, 1991). These compounds have a melting temperature higher than the maximum temperature applied during the solder-reflow process used to connect the electronic components on the printed circuit board (about 260°C). This feature constitutes a great advantage for practical use compared to metallic Li. The LiPON solid electrolyte film, 1.4 µm thick, was then deposited by RF reactive sputtering under pure nitrogen atmosphere. To complete the active part of the microbattery, a metallic lithium film, 3 µm thick, was then deposited on the LiPON film by thermal evaporation. More thorough characterization of similarly prepared solid-state thin film microbatteries has been published in previous studies (Fleutot et al., 2011; Phan et al., 2012; Cras et al., 2015). To protect the active stack from moisture and oxygen, the whole group of 4 cells was capped by a second layer of thin glass. A polymer seal was interposed between the two glass sheets, on the rim of the group of cells to limit the X-ray absorption in this area. The glass substrate was then attached to a rigid printed circuit board and the electrical connection with the cells was achieved using silver-filled epoxy.

In Situ X-Ray Diffraction

High-intensity synchrotron radiation is a necessity to ensure that sufficient intensity can be achieved given the small interaction volume, while allowing for adequate time resolution between each collection. *In situ* X-ray diffraction data were collected in transmission geometry using the Powder Diffraction Beamline at the Australian Synchrotron (Wallwork et al., 2007), using a wavelength of 0.618952(7) Å determined using the NIST 660b LaB_6 standard reference material (Black et al., 2011). The incident beam, with a profile of 1.2 × 3 mm, was focused at the center of a single microbattery cell, see **Figure 1**. Data were collected in the range $5^\circ < 2\theta < 84^\circ$ with collection times of 4 min that were continuously recorded. The microbattery was charged potentiostatically by applying a 0.8 V potential to the cell using a Neware BTS3000 Battery Testing System. Rietveld refinements (Rietveld, 1969) using the *in situ* XRD data were carried out using GSAS-II (Toby and Von Dreele, 2013). Single peak fits were carried out using Gaussian peak shapes with a linear background in LAMP (Richard et al., 1996).

RESULTS AND DISCUSSION

Rietveld Refinement

In order to investigate how the structures of the different phases present within the cell evolve over time, sequential Rietveld refinement of structural models against the collected XRD data was undertaken. Due to the nature of the data, which contains contributions from multiple phases which may exhibit preferred orientation, and background contributions from amorphous phases, it is important to note that several constraints are applied to the data. When carrying out sequential refinement, a number of parameters are refined for only

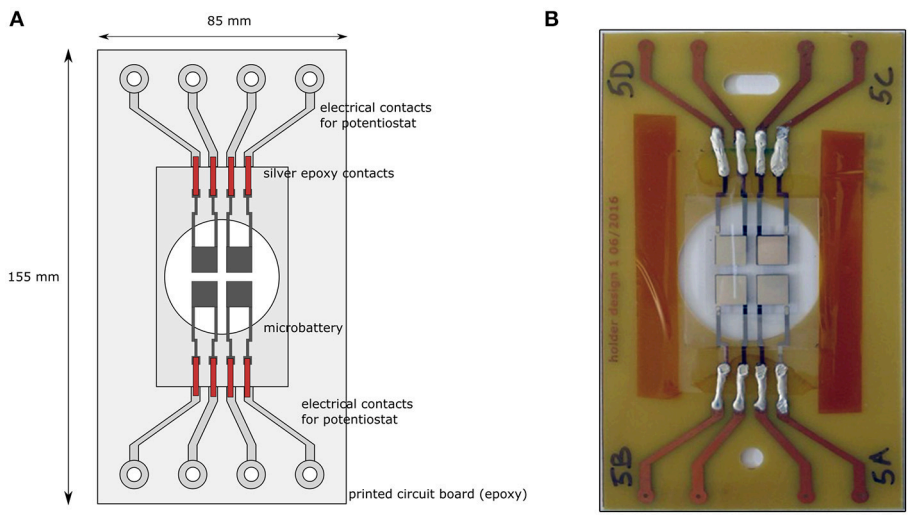

FIGURE 1 | (A) Circuit schematic and **(B)** an example of a printed circuit board with all solid-state microbatteries prepared by sputtering.

one dataset and fixed, while others are allowed to refine throughout the electrochemical process. The fixed parameters include the peak profile parameters, sample parameters, and atomic parameters of the various phases. Peak profile parameters and sample parameters, such as the overall scale factor, sample displacement and sample absorption are fixed as their

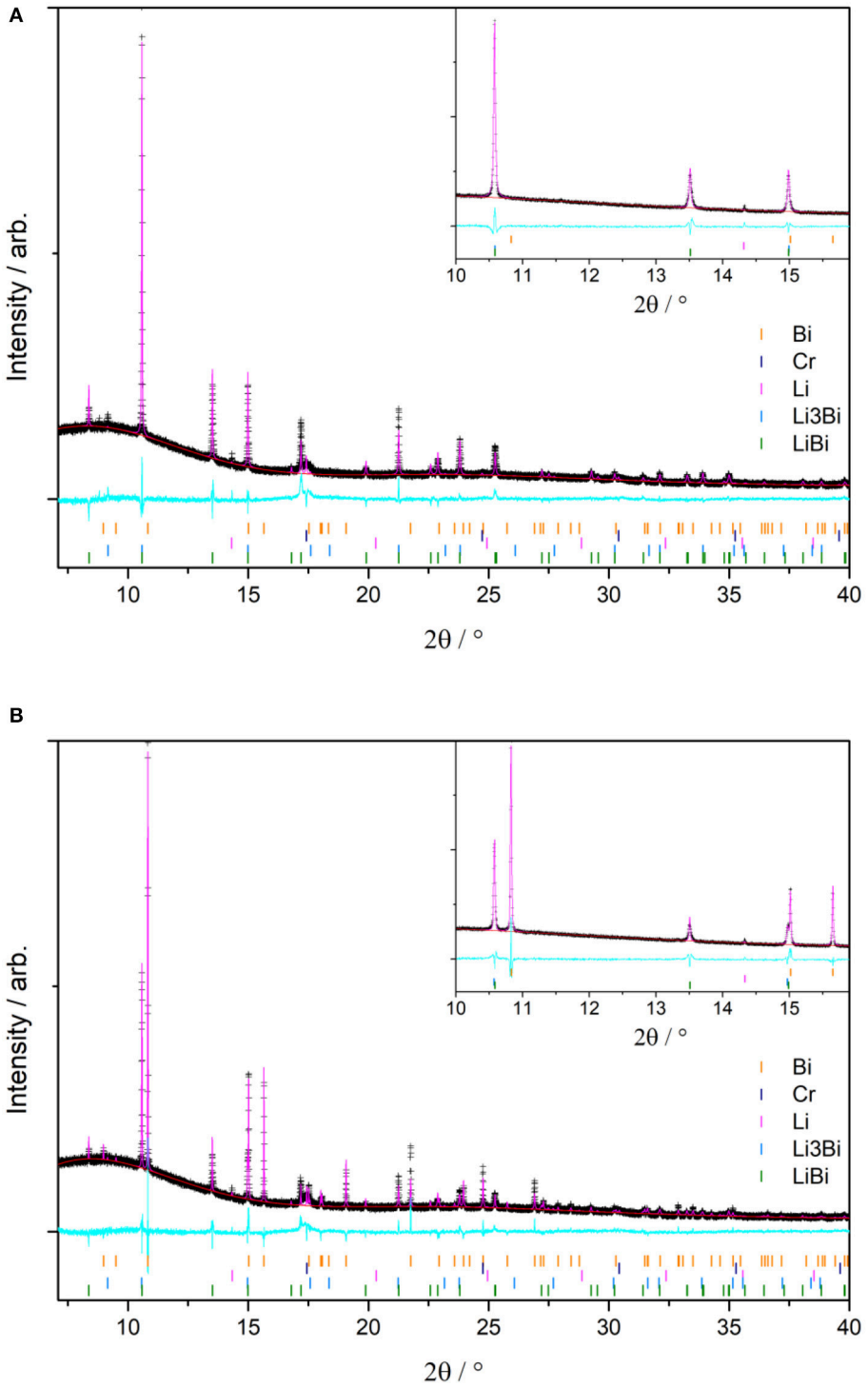

FIGURE 2 | Rietveld refinement profile of the **(A)** first dataset (discharged state) and **(B)** the last dataset (charged state). Reflections from all three major phases are present in the last dataset. Observed data are represented as crosses (+), calculated model as pink line, background function as red line, and difference as cyan line below.

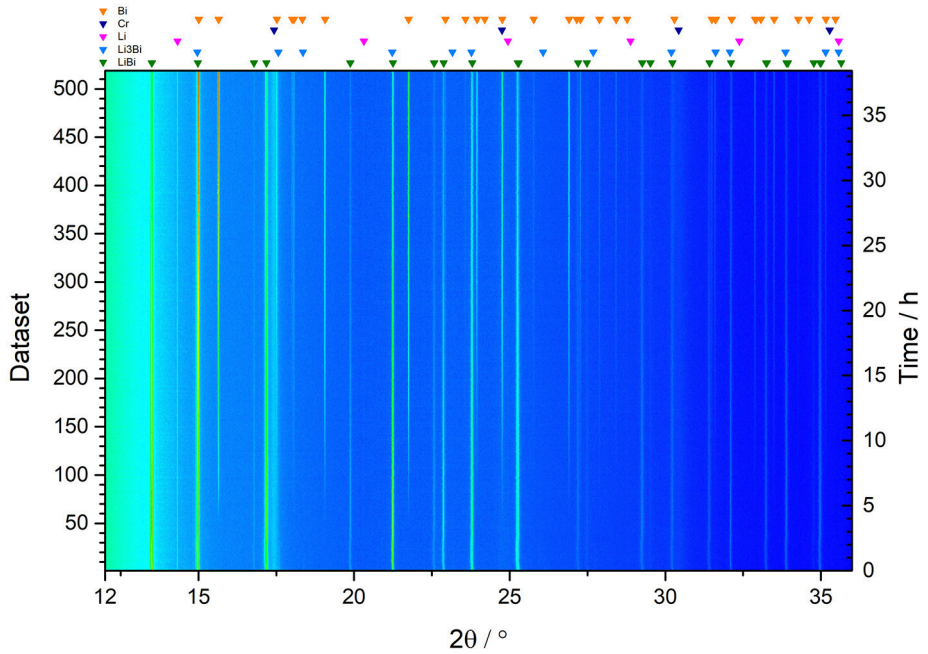

FIGURE 3 | Contour map showing evolution of the collected diffraction data during the 0.8 V potentiostatic hold.

TABLE 1 | Space groups and refined lattice parameters of phases identified in the diffraction data shown in **Figure 2B**.

Phase	Space group	a (Å)	b (Å)	c (Å)	Vol (Å^3)
Bi	*R*−3 *m*	4.54604 (18)	4.54604 (18)	11.86117 (22)	212.287 (12)
LiBi	*P* 4/ *m m m*	3.35667 (8)	3.35667 (8)	4.24097 (19)	47.784 (3)
Li_3Bi	*F m*−3 *m*	6.72065 (25)	6.72065 (25)	6.72065 (25)	303.552 (32)
Li	*I m*−3 *m*	3.50897 (117)	3.50897 (117)	3.50897 (117)	43.205 (43)
Cr	*I m*−3 *m*	2.8881 (2)	2.8881 (2)	2.8881 (2)	24.091 (5)

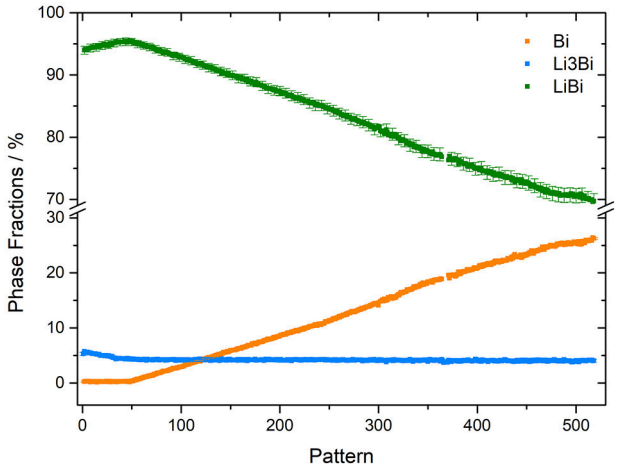

FIGURE 4 | Phase fractions as a function of pattern number as determined by Rietveld refinement.

contributions are known to remain constant throughout the experiment, e.g., the intensity and profile of the incident X-ray beam remain essentially constant, and the sample position relative to the detector remains fixed. Due to the number of phases and low sensitivity of X-rays toward Li, precise structural characterization of the phases present is not possible, and so atomic parameters such as atomic co-ordinates and atomic displacement parameters (ADPs) were fixed. Parameters allowed to refine throughout include the background (Chebyschev function, 13 terms), scale factors for each phase, and structural lattice parameters, apart from Cr and Li which are not expected to undergo expansion/contraction during cycling.

Figures 2A,B show refinements of the first and last datasets, showing the phases present in the discharged and charged state respectively. The observed data is represented by black crosses, while the calculated model is represented by the line through the data. The line below shows the difference between the observed and calculated data. Large spikes in the difference line indicate regions where the least squares refinement approach struggles to model the intensity of particular reflections, in particular the Bi reflection at $2\theta \approx 10.8^\circ$ in **Figure 2B**. The statistics for the refinements shown in **Figures 2A,B** are $wR_p = 7.70\%$ and $wR_p = 9.19\%$, respectively. The wR_p value was found to increase over time, indicating the difficulty in modeling the intensity of the Bi phase which appears as the cell was charged. In this system the discrepancy between the calculated intensity and observed intensity can be attributed primarily

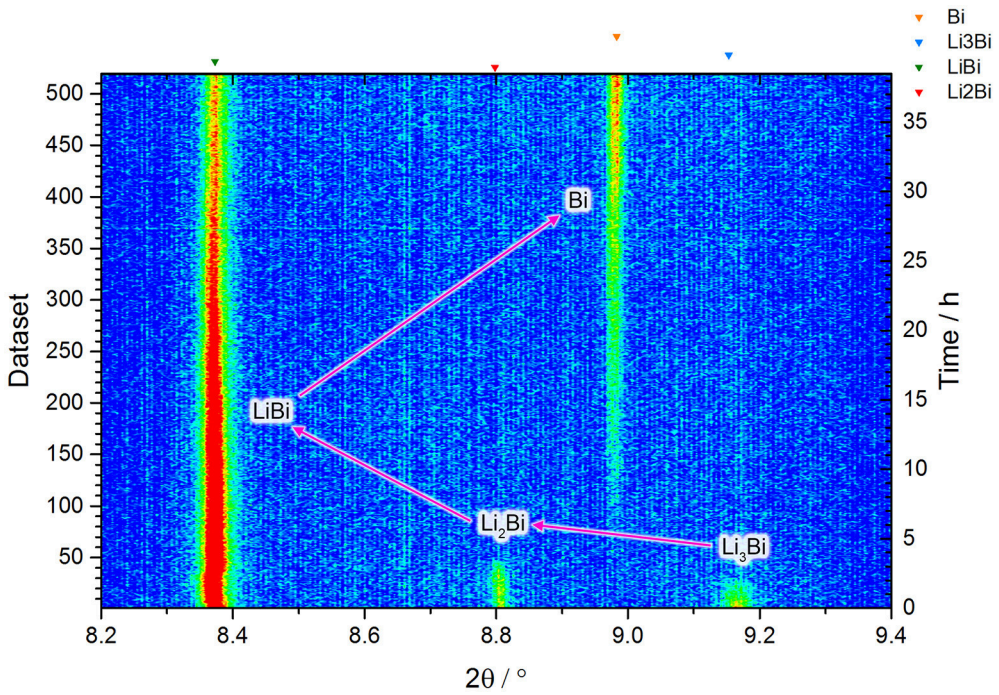

FIGURE 5 | Contour map focusing on the $8.2° < 2\theta < 9.4°$ region, highlighting the range of lithiated bismuth reflections. Arrows indicate a possible reaction pathway.

to two contributions, micro-absorption and sample texturing. Micro-absorption which can arise in systems where there is a large difference in X-ray absorption coefficients between two phases (Taylor and Matulis, 1991), e.g., between Li and Bi in this system. Due to the nature of thin film samples, in which growth of films can occur along particular crystallographic planes, sample texturing can also lead to mismatch between the intensity of calculated models and the observed data for particular reflections (Zolotoyabko, 2009). Sample texturing can be modeled using a preferred orientation model. In this analysis, the strength and direction (along a particular crystallographic plane) of the orientation effects were accounted for using the March-Dollase approach (Von Dreele, 1997). Discrepancies in reflection intensities due to sample texturing can be modeled for each phase individually. Despite "rocking" of the sample stage to improve powder averaging, refinement results suggest strong preferred orientation in the data. It is important to note such contributions which can introduce difficulty in fitting the data, however information about the structural changes taking place within the microbattery such as lattice parameters and phase composition can still be extracted with good confidence. Another consideration to make is that the significant volume expansion often observed during alloying reactions could cause the cell to be displaced relative to the incident beam and affect the cell parameters determined by Rietveld refinement. However, given the nanoscale dimensions of the cell, the magnitude of the volume change is expected to be negligible relative to what would be required to cause issues in the collection of diffraction data, and this is confirmed by the fact that no shift in the position of reflections from the electrochemically inactive cell components is observed during electrochemical cycling.

Structural Evolution

Figure 3 shows the evolution of the diffraction data over time. The alloys formed through electrochemical alloying are known to be identical to those formed metallurgically (Dey, 1971), and in the Li-Bi system. The LiBi and Li_3Bi phases may be formed at ambient temperatures (Zintl and Brauer, 1935; Sangster and Pelton, 1991). In this study, reflections corresponding to the lithiated bismuth phases LiBi, Li_3Bi were observed as well as Bi. Additional reflections can also be seen from the Li metal, and the Cr current collectors, as indicated by the markers above the contour plot. The structures and lattice parameters of the observed phases as determined by Rietveld refinement are detailed in in **Table 1**, and examples of refined fits are shown in **Figure 2**.

The cell was charged potentiostatically at 0.8 V to drive the lithium de-intercalation reactions in the electrode materials. We can observe a series of two-phase reactions occurring. **Figure 4** shows how phase fractions of the three major phases change over time. As the battery is charged, Li is removed from the Bi-Li negative electrode material, resulting in a gradual decrease in the amount of the Li-rich Li_3Bi phase, which reacts to form LiBi, and hence a rapid increase in the amount of LiBi is observed near the beginning of the experiment. As the cell is charged further, the LiBi content begins to decrease and a concurrent increase in the amount of Bi present is observed. A possible reaction pathway is described in **Figure 5**, where we observe reversal of the lithium alloying with Bi via the following

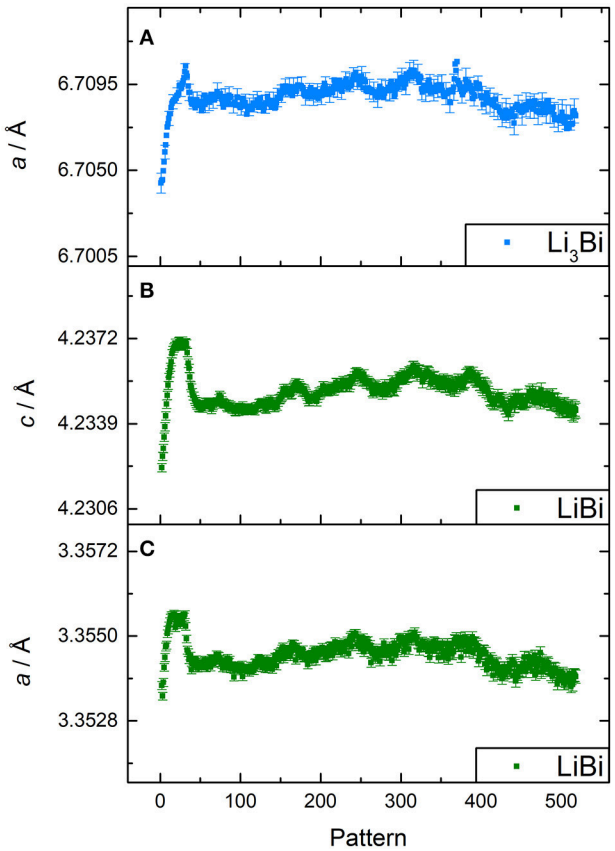

FIGURE 6 | Lattice parameters of the **(A)** Li_3Bi and **(B,C)** LiBi phases as a function of time.

reactions,

$$Li_3Bi \rightarrow LiBi + 2Li^+ + 2e^- \quad (1)$$

$$LiBi \rightarrow Bi + Li^+ + e^- \quad (2)$$

Figure S1 shows an example of a typical charge-discharge curve of a Bi/LiPON/Li all-solid-state cell. The potential profile exhibits two plateaus corresponding to two reactions described above. A similar reaction pathway has been demonstrated for sodium-ion batteries (NIBs) utilizing Bi as a negative electrode material (Gao et al., 2018). The reversibility of the alloying process has been demonstrated previously (Xianming et al., 2002), however it could not be demonstrated during the available beamtime, given the low current densities which thin film batteries were exposed to in this case.

An additional reflection is also observed at $2\theta \approx 8.8^\circ$, see **Figure 5**, resulting from the (1 1 0) plane in Li_2Bi. This Li_2Bi phase forms in small quantities during conversion from Li_3Bi at the discharged state to LiBi during charge. The Li_2Bi structure was recently reported in an amendment to the Li-Bi phase diagram (Pavlyuk et al., 2015). Li_2Bi adopts a hexagonal unit with space group $P-6\ 2\ c$, and in our cell was found to have lattice parameters of $a = 8.061(5)$ Å and $c = 6.835(3)$ Å. In **Figure 5** we also observe reflections corresponding to the (1 1 1), (0 0 1) and (0 0 3) planes of Li_3Bi, LiBi, and Bi respectively.

Closer inspection of the diffraction data in **Figure 5** shows a slight shift in the position of the LiBi 001 reflection ($2\theta \approx 8.37^\circ$) at the beginning of the experiment. Beyond this point, the lattice parameters of the lithiated bismuth phases remain constant, see **Figure 6**, and reaction proceeds via a two-phase mechanism as Bi is formed. The *a* and *c* lattice parameters of LiBi, see **Figures 6B,C**, behave nearly identically as the insertion of lithium into Li_x Bi causes an isotropic expansion of the unit cell.

CONCLUSIONS

The use of *in situ* diffraction to study structural evolution in thin film devices is demonstrated. A series of phase transitions from lithiated bismuth to bismuth metal were identified as the device was charged. This preliminary study of a Bi/LiPON/Li all-solid-state cell demonstrates that these thin film devices can be used to explore the phase transformations which occur within the electrodes during cell operation. Further, the ability to resolve these phase transformations highlights that electrochemical insertion could provide a novel way to explore the phase diagrams of binary alloy systems at ambient temperatures.

AUTHOR CONTRIBUTIONS

DG performed the *in-situ* experiment, analyzed the data and wrote a significant proportion of the manuscript. NS instigated the research and performed the *in-situ* experiment. JK experimental design at the Australian Synchrotron. JG made and tested the *in-situ* cells and designs. BP instigated the research and provided research support throughout the project. FL instigated the research and developed the *in-situ* cell design.

ACKNOWLEDGMENTS

This research was undertaken on the Powder Diffraction beamline at the Australian Synchrotron, Victoria, Australia. DG acknowledges the support of the Australian Government Research Training Program Scholarship. NS would like to thank the Australian Research Council for financial support provided via grants DE160100237 and DP170 100269.

SUPPLEMENTARY MATERIAL

The Supplementary Material for this article can be found online at: https://www.frontiersin.org/articles/10.3389/fenrg.2018.00064/full#supplementary-material

REFERENCES

Bajars, G., Kucinskis, G., Smits, J., and Kleperis, J. (2011). Physical and electrochemical properties of LiFePO 4/C thin films deposited by direct current and radiofrequency magnetron sputtering. *Solid State Ionics* 188, 156–159. doi: 10.1016/j.ssi.2010.10.022

Bang, H. J., Kim, S., and Prakash, J. (2001). Electrochemical investigations of lithium-aluminum alloy anode in Li/polymer cells. *J. Power Sources* 92, 45–49. doi: 10.1016/S0378-7753(00)00522-X

Bates, J. B., Dudney, N. J., Gruzalski, G. R., Zuhr, R. A., Choudhury, A., Luck, C. F., et al. (1992). Electrical properties of amorphous lithium electrolyte thin films. *Solid State Ionics* 53, 647–654. doi: 10.1016/0167-2738(92)90442-R

Bates, J., Dudney, N., Neudecker, B., Ueda, A., and Evans, C. (2000). Thin-film lithium and lithium-ion batteries. *Solid State Ionics* 135, 33–45. doi: 10.1016/S0167-2738(00)00327-1

Bates, J., Gruzalski, G., Dudney, N., Luck, C., and Yu, X. (1994). Rechargeable thin-film lithium batteries. *Solid State Ionics* 70, 619–628. doi: 10.1016/0167-2738(94)90383-2

Besenhard, J., Yang, J., and Winter, M. (1997). Will advanced lithium-alloy anodes have a chance in lithium-ion batteries? *J. Power Sources* 68, 87–90. doi: 10.1016/S0378-7753(96)02547-5

Black, D. R., Windover, D., Henins, A., Filliben, J., and Cline, J. P. (2011). Certification of standard reference material 660B. *Powder Diffract.* 26, 155–158. doi: 10.1154/1.3591064

Cras, F. L., Pecquenard, B., Dubois, V., Phan, V.-P., and Guy-Bouyssou, D. (2015). All-solid-state lithium-ion microbatteries using silicon nanofilm anodes: high performance and memory effect. *Adv. Energy Mater.* 5:1501061. doi: 10.1002/aenm.201501061

Crosnier, O., Brousse, T., Devaux, X., Fragnaud, P., and Schleich, D. (2001). New anode systems for lithium ion cells. *J. Power Sources* 94, 169–174. doi: 10.1016/S0378-7753(00)00599-1

Dey, A. (1971). Electrochemical alloying of lithium in organic electrolytes. *J. Electrochem. Soc.* 118, 1547–1549. doi: 10.1149/1.2407783

Dimov, N. (2009). "Development of metal alloy anodes," in *Lithium-Ion Batteries,* eds Em. M. Yoshio, A. Kozawa, and R. J. Brodd (New York, NY: Springer), 241–265. doi: 10.1007/978-0-387-34445-4_11

Dudney, N. J. (2005). Solid-state thin-film rechargeable batteries. *Mater. Sci. Eng.* 116, 245–249. doi: 10.1016/j.mseb.2004.05.045

Dudney, N. J., and Neudecker, B. J. (1999). Solid state thin-film lithium battery systems. *Curr. Opin. Solid State Mater. Sci.* 4, 479–482. doi: 10.1016/S1359-0286(99)00052-2

Fleutot, B., Pecquenard, B., Le Cras, F., Delis, B., Martinez, H., Dupont, L., et al. (2011). Characterization of all-solid-state Li/LiPONB/TiOS microbatteries produced at the pilot scale. *J. Power Sour.* 196, 10289–10296. doi: 10.1016/j.jpowsour.2011.07.018

Gao, H., Ma, W., Yang, W., Wang, J., Niu, J., Luo, F., et al. (2018). Sodium storage mechanisms of bismuth in sodium ion batteries: an operando X-ray diffraction study. *J. Power Sour.* 379, 1–9. doi: 10.1016/j.jpowsour.2018.01.017

Gong, Y., Zhang, J., Jiang, L., Shi, J.-A., Zhang, Q., Yang, Z., et al. (2017). *In situ* atomic-scale observation of electrochemical delithiation induced structure evolution of LiCoO2 cathode in a working all-solid-state battery. *J. Am. Chem. Soc.* 139, 4274–4277. doi: 10.1021/jacs.6b13344

Goonetilleke, D., Pramudita, J. C., Hagan, M., Al Bahri, O. K., Pang, W. K., Peterson, V. K., et al. (2017). Correlating cycling history with structural evolution in commercial 26650 batteries using in operando neutron powder diffraction. *J. Power Sour.* 343, 446–457. doi: 10.1016/j.jpowsour.2016.12.103

Gustafsson, T., Thomas, J. O., Koksbang, R., and Farrington, G. C. (1992). The polymer battery as an environment for *In Situ* X-ray diffraction studies of solid-state electrochemical processes. *Electrochim. Acta* 37, 1639–1643. doi: 10.1016/0013-4686(92)80128-9

Hu, C.-W., Sharma, N., Chiang, C.-Y., Su, H.-C., Peterson, V. K., Hsieh, H.-W., et al. (2013). Real-time investigation of the structural evolution of electrodes in a commercial lithium-ion battery containing a V-added LiFePO4 cathode using *In-Situ* neutron powder diffraction. *J. Power Sour.* 244, 158–163. doi: 10.1016/j.jpowsour.2013.02.074

Huggins, R. A. (1999). Lithium alloy negative electrodes. *J. Power Sour.* 81–82, 13–19. doi: 10.1016/S0378-7753(99)00124-X

Jacke, S., Song, J., Cherkashinin, G., Dimesso, L., and Jaegermann, W. (2010). Investigation of the solid-state electrolyte/cathode LiPON/LiCoO2 interface by photoelectron spectroscopy. *Ionics* 16, 769–775. doi: 10.1007/s11581-010-0479-1

Jones, S. D., Akridge, J. R., and Shokoohi, F. K. (1994). Thin film rechargeable Li batteries. *Solid State Ionics* 69, 357–368. doi: 10.1016/0167-2738(94)90423-5

Kanehori, K., Matsumoto, K., Miyauchi, K., and Kudo, T. (1983). Thin film solid electrolyte and its application to secondary lithium cell. *Solid State Ionics* 9, 1445–1448. doi: 10.1016/0167-2738(83)90192-3

Ma, C., Cheng, Y., Yin, K., Luo, J., Sharafi, A., Sakamoto, J., et al. (2016). Interfacial Stability of Li metal–solid electrolyte elucidated via *in situ* electron microscopy. *Nano Lett.* 16, 7030–7036. doi: 10.1021/acs.nanolett.6b03223

Massalski, T. B., Okamoto, H., Subramanian, P., Kacprzak, L., and Scott, W. W. (1986). *Binary Alloy Phase Diagrams*. Metals Park, OH: American Society for Metals.

Neudecker, B., Dudney, N., and Bates, J. (2000). "Lithium-free" thin-film battery with *in situ* plated li anode. *J. Electrochem. Soc.* 147, 517–523. doi: 10.1149/1.1393226

Oudenhoven, J., Labohm, F., Mulder, M., Niessen, R., Mulder, F., and Notten, P. (2011). *In situ* neutron depth profiling: a powerful method to probe lithium transport in micro-batteries. *Adv. Mater.* 23, 4103–4106. doi: 10.1002/adma.201101819

Pang, W. K., Kalluri, S., Peterson, V. K., Sharma, N., Kimpton, J., Johannessen, B., et al. (2015). Interplay between electrochemistry and phase evolution of the P2-type Na x (Fe1/2Mn1/2) O2 cathode for use in sodium-ion batteries. *Chem. Mater.* 27, 3150–3158. doi: 10.1021/acs.chemmater.5b00943

Pavlyuk, V., Sozanskyi, M., Dmytriv, G., Indris, S., and Ehrenberg, H. (2015). Amendment of the Li-Bi phase diagram crystal and electronic structure of Li2Bi. *J. Phase Equilib. Diffus.* 36, 544–553. doi: 10.1007/s11669-015-0409-z

Pecquenard, B., Le Cras, F. D. R., Poinot, D., Sicardy, O., and Manaud, J.-P. (2014). Thorough characterization of sputtered CuO thin films used as conversion material electrodes for lithium batteries. *ACS Appl. Mater. Interfaces* 6, 3413–3420. doi: 10.1021/am4055386

Pelé, V., Flamary, F., Bourgeois, L., Pecquenard, B., and Le Cras, F. (2015). Perfect reversibility of the lithium insertion in FeS 2: the combined effects of all-solid-state and thin film cell configurations. *Electrochem. Commun.* 51, 81–84. doi: 10.1016/j.elecom.2014.12.009

Phan, V. P., Pecquenard, B., and Le Cras, F. (2012). High-performance all-solid-state cells fabricated with silicon electrodes. *Adv. Funct. Mater.* 22, 2580–2584. doi: 10.1002/adfm.201200104

Richard, D., Ferrand, M., and Kearley, G. (1996). Lamp, the large array manipulation program. *J. Neutron Res.* 4, 33–39. doi: 10.1080/10238169608200065

Rietveld, H. (1969). A profile refinement method for nuclear and magnetic structures. *J. Appl. Crystallogr.* 2, 65–71. doi: 10.1107/S0021889869006558

Sangster, J., and Pelton, A. (1991). The Bi-Li (Bismuth-Lithium) system. *J. Phase Equilibria* 12, 447–450. doi: 10.1007/BF02645966

Senevirathne, K., Day, C. S., Gross, M. D., Lachgar, A., and Holzwarth, N. A. W. (2013). A new crystalline LiPON electrolyte: synthesis, properties, and electronic structure. *Solid State Ionics* 233, 95–101. doi: 10.1016/j.ssi.2012.12.013

Sharma, N., Gonzalo, E., Pramudita, J. C., Han, M. H., Brand, H. E. A., Hart, J. N., et al. (2015a). The unique structural evolution of the O3-phase Na2/3Fe2/3Mn1/3O2during high rate charge/discharge: a sodium-centred perspective. *Adv. Funct. Mater.* 25, 4994–5005. doi: 10.1002/adfm.201501655

Sharma, N., Pang, W. K., Guo, Z., and Peterson, V. K. (2015b). *In situ* powder diffraction studies of electrode materials in rechargeable batteries. *ChemSusChem.* 8, 2826–2853. doi: 10.1002/cssc.201500152

Sharma, N., and Peterson, V. K. (2012). *In situ* neutron powder diffraction studies of lithium-ion batteries. *J. Solid State Electrochem.* 16, 1849–1856. doi: 10.1007/s10008-011-1567-5

Takada, K. (2013). Progress and prospective of solid-state lithium batteries. *Acta Mater.* 61, 759–770. doi: 10.1016/j.actamat.2012.10.034

Taylor, J., and Matulis, C. (1991). Absorption contrast effects in the quantitative XRD analysis of powders by full multiphase profile refinement. *J. Appl. Crystallogr.* 24, 14–17. doi: 10.1107/S002188989000841X

Teng, S., Tan, J., and Tiwari, A. (2014). Recent developments in garnet based solid state electrolytes for thin film batteries. *Curr. Opin. Solid State Mater. Sci.* 18, 29–38. doi: 10.1016/j.cossms.2013.10.002

Toby, B. H., and Von Dreele, R. B. (2013). GSAS-II: the genesis of a modern open-source all purpose crystallography software package. *J. Appl. Crystallogr.* 46, 544–549. doi: 10.1107/S0021889813003531

Von Dreele, R. (1997). Quantitative texture analysis by Rietveld refinement. *J. Appl. Crystallogr.* 30, 517–525. doi: 10.1107/S0021889897005918

Wallwork, K. S., Kennedy, B. J., and Wang, D. (2007). "The high resolution powder diffraction beamline for the Australian Synchrotron," in *AIP Conference Proceedings: AIP* (Clayton), 879–882. doi: 10.1063/1.2436201

Wang, C., Gong, Y., Dai, J., Zhang, L., Xie, H., Pastel, G., et al. (2017). *In situ* neutron depth profiling of lithium metal–garnet interfaces for solid state batteries. *J. Am. Chem. Soc.* 139, 14257–14264. doi: 10.1021/jacs.7b07904

Wang, Z., Santhanagopalan, D., Zhang, W., Wang, F., Xin, H. L., He, K., et al. (2016). *In situ* STEM-EELS observation of nanoscale interfacial phenomena in all-solid-state batteries. *Nano Lett.* 16, 3760–3767. doi: 10.1021/acs.nanolett.6b01119

Wen, C. J., and Huggins, R. A. (1981). Chemical diffusion in intermediate phases in the lithium-silicon system. *J. Solid State Chem.* 37, 271–278. doi: 10.1016/0022-4596(81)90487-4

West, K., Zachau-Christiansen, B., Skaarup, S., and Poulsen, F. (1992). Lithium insertion in sputtered vanadium oxide film. *Solid State Ionics* 57, 41–47. doi: 10.1016/0167-2738(92)90062-T

Xia, H., Meng, Y., Lu, L., and Ceder, G. (2007). Electrochemical properties of nonstoichiometric LiNi0. 5Mn1. 5O4– δ thin-film electrodes prepared by pulsed laser deposition. *J. Electrochem. Soc.*154, A737–A743. doi: 10.1149/1.2741157

Xianming, W., Nishina, T., and Uchida, I. (2002). Lithium alloy formation at bismuth thin layer electrode and its kinetics in propylene carbonate electrolyte. *J. Power Sour.* 104, 90–96. doi: 10.1016/S0378-7753(01)00876-X

Yao, N., Heredy, L., and Saunders, R. (1971). Emf measurements of electrochemically prepared lithium-aluminum alloy. *J. Electrochem. Soc.* 118, 1039–1042. doi: 10.1149/1.2408242

Yoon, Y., Park, C., Kim, J., and Shin, D. (2013). Lattice orientation control of lithium cobalt oxide cathode film for all-solid-state thin film batteries. *J. Power Sour.* 226, 186–190. doi: 10.1016/j.jpowsour.2012.10.094

Zhang, W.-J. (2011). A review of the electrochemical performance of alloy anodes for lithium-ion batteries. *J. Power Sour.* 196, 13–24. doi: 10.1016/j.jpowsour.2010.07.020

Zhao, Y., Li, X., Yan, B., Li, D., Lawes, S., and Sun, X. (2015). Significant impact of 2D graphene nanosheets on large volume change tin-based anodes in lithium-ion batteries: a review. *J. Power Sour.* 274, 869–884. doi: 10.1016/j.jpowsour.2014.10.008

Zhou, Y.-N., Xue, M.-Z., and Fu, Z.-W. (2013). Nanostructured thin film electrodes for lithium storage and all-solid-state thin-film lithium batteries. *J. Power Sour.* 234, 310–332. doi: 10.1016/j.jpowsour.2013.01.183

Zintl, E., and Brauer, G. (1935). Konstitution der lithium-wismut-legierungen: 14. mitteilung über metalle u. legierungen. *Berichte Bunsengesellschaft Physikalische Chemie* 41, 297–303.

Zolotoyabko, E. (2009). Determination of the degree of preferred orientation within the March–Dollase approach. *J. Appl. Crystallogr.* 42, 513–518. doi: 10.1107/S0021889809013727

Conflict of Interest Statement: The authors declare that the research was conducted in the absence of any commercial or financial relationships that could be construed as a potential conflict of interest.